JOURNAL OF MATERIALS SCIENCE **40** (2005) 5191 – 5198

Effect of inclusion size on mechanical properties of alumina toughened cubic zirconia

MIROSŁAW M. BUĆKO, WALDEMAR PYDA
AGH University of Science and Technology, Faculty of Materials Science and Ceramics, Mickiewicza Av. 30, 30-059 Cracow, Poland
E-mail: bucko@uci.agh.edu.pl

The relationship between alumina inclusion size and mechanical properties of particulate cubic zirconia-alumina composites was studied. The composites of the diverse size and content of alumina inclusions and of the nearly constant size of zirconia grains were used. Physical mixtures of the 8 mol% Y_2O_3-ZrO_2 nano-powder and the γ-Al_2O_3 or α-Al_2O_3 micro-powder were cold isostatically pressed and then pressurelessly sintered for 2 h at 1300°C in air. The γ-Al_2O_3 and α-Al_2O_3 powder was composed of the particles of 0.17 and 0.36 μm in size, respectively. Crystallites of the zirconia powder had the size of 6 nm. Microstructural features of the composites have been characterised quantitatively. Hardness, critical stress intensity factor and bending strength of the composites was measured and correlated with the microstructural features. Depending on the size and content, the alumina inclusions influenced strength of the composites by influencing their fracture toughness and the presence of flaws of critical size. An increase in size of the alumina inclusions was accompanied by the increase of fracture toughness due to the additional contribution of large alumina inclusions to the crack deflection mechanism. It was found that decreasing the alumina inclusion size significantly below the cubic zirconia matrix grain size (more than 3 times) did not lead to the increased values of fracture toughness of the composites. The highest increase in fracture toughness (up to 3.9 MPa·m$^{0.5}$) has been found when the inclusion size was comparable to the matrix grain size.

1. Introduction

As an important representative of functional ceramics, cubic zirconia doped with yttria (CSZ) is extensively used in many applications e.g.: in probes for the oxygen partial pressure measurements, oxygen pumps or solid oxide fuel cells. This is due to its low electronic and high oxygen ion conductivity, excellent chemical stability under reduced and oxidised atmosphere at a high temperature, and relatively low production costs. A certain limitation arises from its moderate mechanical strength and fracture toughness. For example, the solid oxide full cell requirements for electrolytes, which are: a bending strength of $\sigma_f \geq 500$ MPa and a fracture toughness of $K_{\mathrm{Ic}} \geq 3$ MPa $\cdot$ m$^{0.5}$ [1], can not be satisfied by the ordinary CSZ. The incorporation of inert inclusions into the cubic zirconia matrix is a common way of improvement both mechanical and electrical properties of the material [2–10]. The alumina inclusions are the most frequently utilised. The improved electrical characteristics of the cubic zirconia-alumina particulate composites are generally attributed to the interaction between alumina and silica which modifies interfaces and grain boundaries as a result of purifying them from the silica reach glassy phase [2]. The improved mechanical properties are related to toughening mechanisms that involve alteration of crack paths by means of stress fields from mismatches in the thermal and elastic constants of the alumina and zirconia phases, such that the net crack-driving force is reduced. Crack deflection and crack bridging has been found to operate in cubic zirconia-alumina composites.

The influence of alumina addition on microstructure and mechanical properties of the cubic zirconia—Al_2O_3 particulate composites was extensively studied [3, 6–11]. In the most cases, studies concerned on optimisation of the amount of alumina inclusions incorporated into the composite and a fabrication method applied with respect to the properties obtained. An increase of bending strength accompanied by a decrease of electrical conductivity with increasing alumina content up to 20 wt% has been reported [3, 7]. Further alumina addition was not effective for strengthening when up to 8 mol% yttria for stabilising cubic zirconia and pressureless sintering in air has been applied. The utilization of increased amounts of stabilizing yttria (10 mol%) and hot pressing as a densification method enabled reaching a maximum of flexural strength and fracture toughness at 24.7 wt% of alumina [11]. The spectacular increase of flexural strength, up to 480 MPa, without changes of ionic conductivity has been

0022–2461
DOI: 10.1007/s10853-005-4412-3

obtained in the cubic zirconia reinforced with 24.7 wt% alumina as a result of suitable modification of the composite microstructure by means of pressureless sintering at a rapid heating rate of $820^{\circ}C \cdot h^{-1}$ [9].

There have been relatively few studies examining the relation between alumina inclusion size and mechanical properties of the alumina-cubic zirconia composites. Mori *et al*. [7] examined cubic zirconia composites containing alumina particles ranging from 0.23 to 0.68 μm. The strength of the composites sintered for 4 h at 1600°C was not affected significantly by Al_2O_3 particle size and its influence on fracture toughness was not studied. In the aforesaid work by Oe *et al*. [9] the alumina particles of 0.38 μm have been found more suitable for the production of cubic zirconia-alumina composites with improved mechanical properties than those of 3 μm in size.

The current contribution describes a detailed microstructural investigation to determine the effect of alumina inclusion size on hardness, fracture toughness and bending strength of the alumina-cubic zirconia composites. The composites that contained the alumina inclusions of diverse size (also near-nanometric one) homogeneously dispersed in the zirconia matrix of the constant grain size were used.

2. Experimental

A method which utilises physical mixtures of a cubic zirconia nano-powder and a suitable alumina powder has been chosen for the preparation of composite materials of controlled microstructure.

The hydrothermal crystallisation of a co-precipitated yttria-zirconia hydrogel was used as a method of preparation of the zirconia nano-powder which contained 8 mol% Y_2O_3 in solid solution [12]. First, an aqueous solution of zirconium and yttrium chlorides of a concentration of $\sim 2\ mol \cdot dm^{-3}$ was prepared. Then the small doses of it were introduced to a vigorously stirred ammonia aqueous solution (1:1). The co-precipitated hydrogel was washed with distilled water by means of decantation and filtration in order to remove chlorine ions. Then it was hydrothermally treated for 4 h at 240°C under an autogeneous pressure of saturated water vapour. The crystalline zirconia powder was additionally heat treated for 30 min at 400°C.

Two alumina powders were used to produce the inclusions of diverse size in the composites. The first one was a fine γ-Al_2O_3 powder which was derived from an alum method. The second one was a coarse grained α-Al_2O_3 powder which was obtained through the calcination of the aforementioned γ-Al_2O_3 powder for 1 h at 1300°C. The zirconia powder was physically mixed with each of the alumina powder in order to prepare homogeneous mixtures containing up to 15 wt% alumina. A rotary-vibratory mill, Y-TZP grinding media, ethyl alcohol environment and a homogenisation time of 15 min were used. One percent additive of oleic acid was incorporated into each mixture as a lubricant. The mixtures were dried at the room temperature, granulated and then they were cold isostatically pressed under a pressure of 200 MPa. The green compacts were pressurelessly sintered for 2 h at 1300°C in air. During heating, the samples were kept for 30 min. at 450°C in order to remove oleic acid.

Within the whole text, the specimens derived from the α-Al_2O_3 powder are marked as A*n* and those prepared from the γ-Al_2O_3 one as G*n*, where *n* denotes weight fraction of aluminium oxide in the composite.

The crystallite size of the starting powders, $d_{(hkl)}$, was assessed from X-ray line broadening. A (111) peak of cubic zirconia, (400) of γ-Al_2O_3 and (012) α-Al_2O_3 was analysed, respectively. The specific surface area of the powders was measured by the one point BET method. The samples were outgased at 150°C in vacuum. The results were used to calculate an equivalent particle size, d_{BET}. The apparent density of the composites was measured by the Archimedes method and their phase composition by X-ray diffraction analysis.

A numerical analysis of SEM microphotographs (VisiLog 4 program – Noesis), taken from the polished and thermally etched surfaces, was applied to measure microstructural parameters quantitatively.

Hardness, *HV*, and fracture toughness, K_{Ic}, of the composites was determined on polished surfaces by Vickers' indentation. A loading force of 49.05 N imposed by 10 s was applied. The Palmqvist crack model was used [13] to calculate K_{Ic}. Bending strength of the samples of $4 \times 4 \times 45$ mm in size was measured by the three-point method, using a distance between support rollers of 40 mm and a loading rate of $2\ mm \cdot min^{-1}$.

3. Results and discussion

Basic characteristics of the starting powders are shown in Table I. The values of equivalent particle size, d_{BET}, lay very close to those of crystallite size, $d_{(hkl)}$, for both the ZrO_2 and γ-Al_2O_3 powders. This indicates not extensive contacts between primary particles of the two powders and is promising for existence of rather weak agglomerates. The α-Al_2O_3 micro-powder contained the particles that were on average about two times bigger than those of the γ-Al_2O_3 micro-powder. The stronger agglomerates of the α-Al_2O_3 micro-powder are suggested by the relatively high synthesis temperature. The ZrO_2 powder was a nanometric one. It was composed of isometric crystallites of ~6 nm in size and cubic symmetry. A crystallite size distribution was very narrow as confirmed by the TEM observations.

No other phases than the cubic zirconia and alpha alumina were found in X-ray diffraction patterns of the sintered materials both of *A* and *G* series.

Fig. 1 shows an effect of the alumina inclusions content on apparent density of the composites studied. An increase of the alumina content caused the deterioration of sinterability of the composite powders. This results from the shrinkage incompatibilities of the

TABLE I Specific surface area, S_{BET}, equivalent particle size, d_{BET}, and crystallite size, d_{hkl}, of the starting powders

	ZrO_2	γ-Al_2O_3	$\alpha - Al_2O_3$
S_{BET} (m^2/g)	156.2 ± 1.0	8.8 ± 0.9	4.2 ± 0.6
d_{BET} (nm)	6.4 ± 0.1	171 ± 2	357 ± 12
$d_{(hkl)}$ (nm)	5.8 ± 0.3	155 ± 9	>200

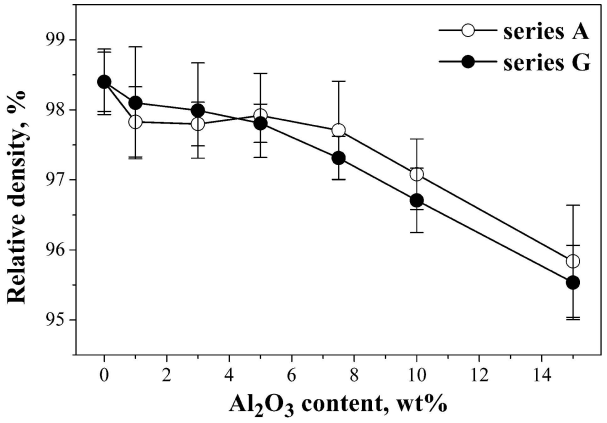

Figure 1 Compositional dependence of relative density of the sintered bodies.

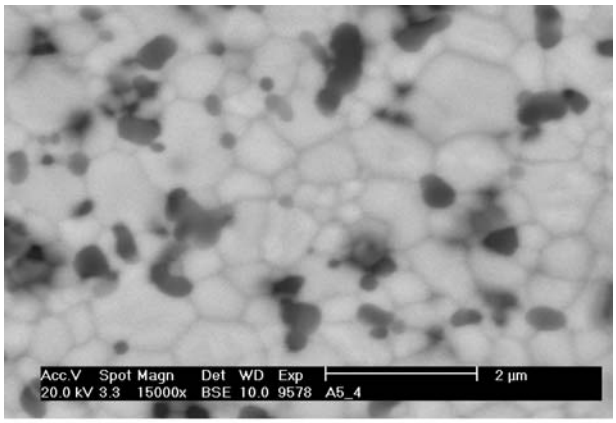

(a)

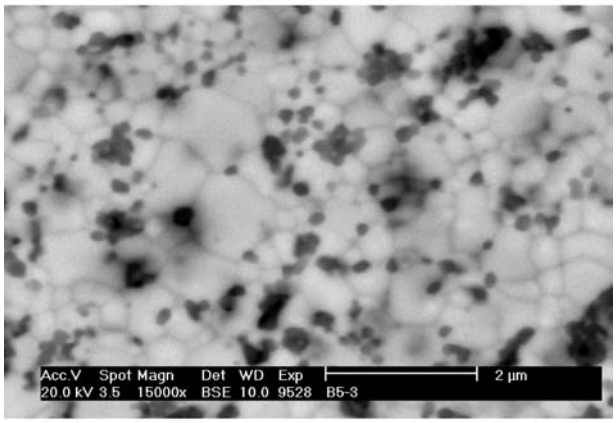

(b)

Figure 2 SEM microphotographs of the microstructure of the cubic zirconia containing 10 wt% of alumina inclusions: (a) series A; (b) series G.

matrix and the inclusion during densification. The plausible hypotheses about the phenomena underlying the retardation of pressureless densification by elastic inclusions are as follows. The early proposal concerns the suppression of densification by the hydrostatic tensile stresses that develop in the porous matrix around the inclusions [14–19]. Another proposal suggests that the interaction of nontouching inclusions inhibits contraction of the matrix interstices and predicts that matrix densification is heterogeneous [20, 21]. It was demonstrated [22] that salient aspects of both proposals are involved and interact to produce retardation. The suppressed grain growth of the matrix grains during sintering is also considered as a factor of the retarded densification of particulate composites [23, 24]. The inclusions inhibit grain boundary migration and therefore they inhibit grain growth which is needed for removing porosity. According to the model proposed by Kellet and Lange [25, 26], grain growth is the essential condition for the changes of pore geometry due to the disappearance of some neighbouring grains. In such a case the pore interfaces become convex and the pore can shrink spontaneously.

The retarding effect of alumina increased with decreasing particle size at the inclusion content larger than 5 wt% (Fig. 1). This is consistent with the observations reported by Weiser *et al.* [27] for ZnO containing dispersed SiC particles.

The SEM observations revealed Al_2O_3 particulates dispersed mainly at grain boundaries (typical images are shown in Fig. 2). Some inclusions of the smallest size have been found at within zirconia matrix grains. This behaviour is attributed to the interaction between the pinning force by one particle which depends on its size and the driving force for grain boundary migration [28]. The distorted grain boundaries of the zirconia matrix accompanied the presence of alumina particles at the grain boundaries, while grain boundaries of cubic zirconia with any inclusions were not distorted, as shown in Fig. 2.

Grain size distributions of the zirconia matrix as a function of alumina content of both series *A* and *G* are shown in Fig. 3a and b, respectively. Figs 3c and d shows the related alumina inclusion size distributions. The nominal grain or inclusion size which appears in the distribution denotes the diameter of a circle having area equal to that of the measured grain cross-section. Fig. 4 shows arithmetical average sizes of the matrix grain and the inclusion as a function of the alumina content in the composite. The interval of variability denotes a standard deviation which was used as a measure of dispersion of the particle size.

Both the zirconia grain and alumina inclusion size distributions in the studied composites were monomodal, relatively narrow and typically broadened towards the bigger and bigger grains (Fig. 3). The zirconia grain size distributions of both series of the composites became narrower and narrower with an increase of the alumina content. Simultaneously the average zirconia grain size decreased (Figs 3 and 4).

It is evident from the presented results that grain boundary migration was inhibited by alumina particles. As one can calculate from the data of Fig. 4b, number of inclusions per volume unit is larger in the composites derived from the fine-grained alumina powder (*G* series) than in those derived from the coarse-grained powder (*A* series) when composites with the same alumina content are compared. This is the reason for more effective blocking grain boundary movement by the alumina inclusions in the composites of the *G* series than those of the A one which contained larger than 3 wt% alumina and therefore clearly smaller grain size of the matrix in the former composites. The presented findings are consistent with predictions of Zener's formula

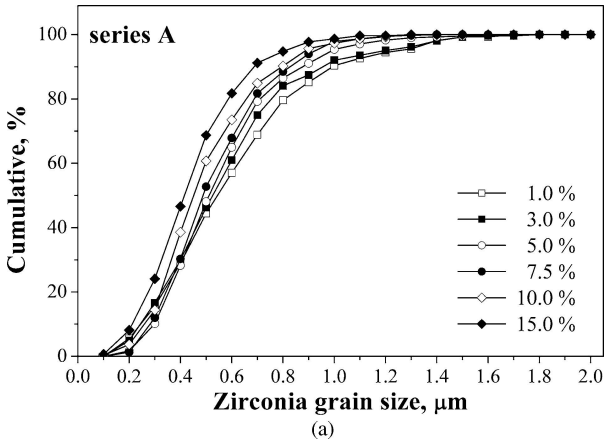

(a)

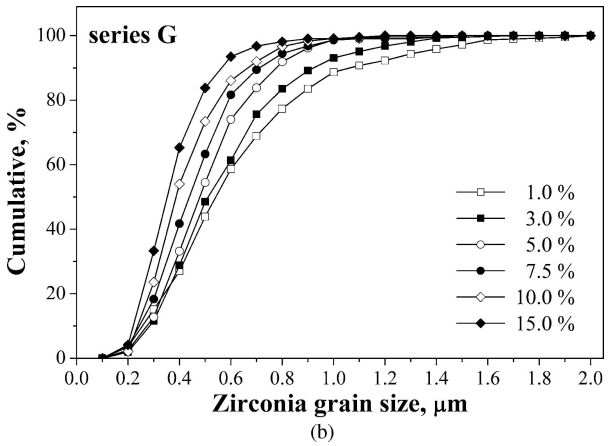

(b)

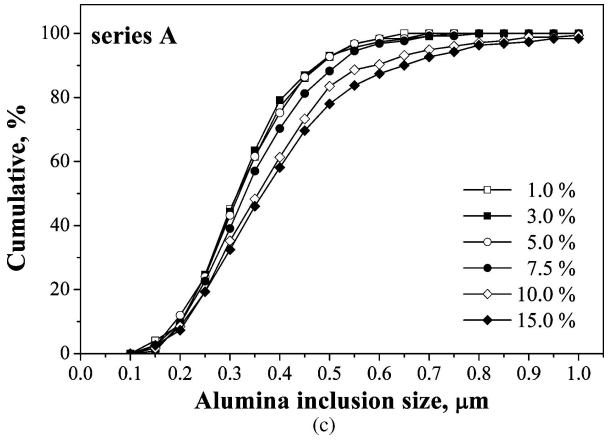

(c)

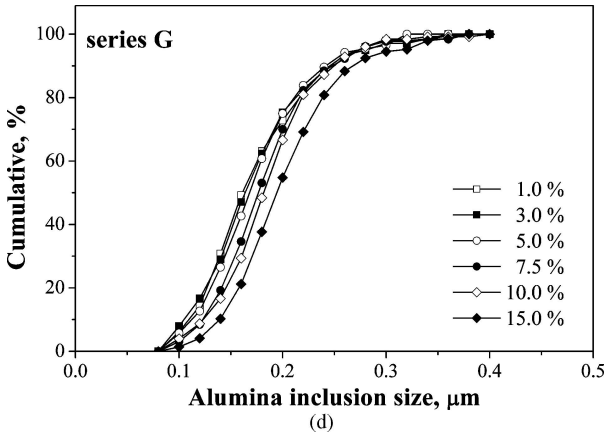

(d)

Figure 3 Zirconia matrix grain size distributions: (a) series A, (b) series G, and alumina inclusion size distributions: (c) series A, (d) series G as a function of alumina content in the composite.

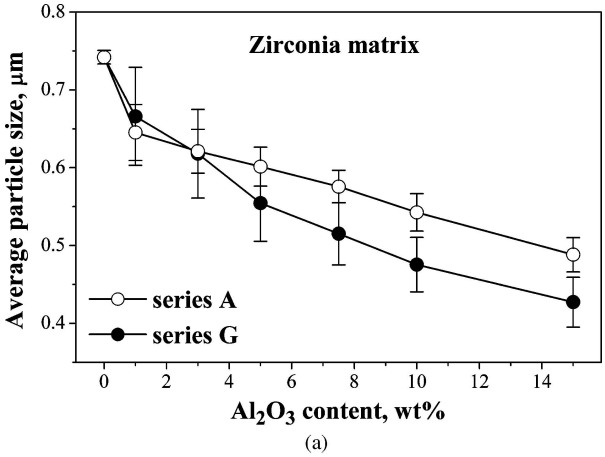

(a)

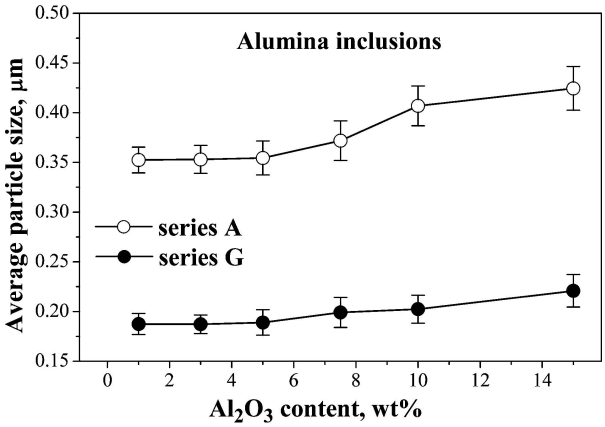

(b)

Figure 4 Compositional dependence of an average particle size of the sintered bodies: (a) matrix grains, (b) inclusions.

which suggests that mean grain size (G) decreases with increasing volume fraction of the second phase (f) and with decreasing mean inclusion size (r) [29]:

$$G = k\frac{r}{f} \tag{1}$$

where k is constant. The effect of suppressing the growth of zirconia grains during sintering by addition of alumina was also reported by other researchers [e.g. 3, 7, 8, 23, 30].

The opposite tendency was observed in the case of relationship between the alumina inclusion size and the alumina content in the zirconia composites (Fig. 4b). The increase of the alumina inclusions content was accompanied by moderate increase of their size and the distribution width. It is supposed that the reason is connected with the processes that led to the formation of clusters of alumina particles on the powder mixture preparation stage. Coagulation of individual particles of aluminium oxide in the ethyl alcohol environment during homogenisation of the powder mixtures in the rotary-vibratory mill could be such a process. The probability of connection of the Al_2O_3 particles each other, and so, the probability of the agglomerate formation, increases with the increase of Al_2O_3 content. After sintering, this results in the inclusions enlarged the more, the larger is the alumina content.

The results of statistical analysis of the values of shape coefficient and Feret diameter, shown in Table II,

TABLE II Mean value of parameters chosen to characterize the microstructure of the composites

Al_2O_3 (%)	Shape coefficient[a]	Feret diameter X (μm)	Feret diameter Y (μm)	Shape coefficient[a]	Feret diameter X (μm)	Feret diameter Y (μm)
		A series—ZrO_2 matrix			A series—Al_2O_3 inclusions	
1	1.28 ± 0.02	0.61 ± 0.04	0.70 ± 0.04	1.16 ± 0.06	0.28 ± 0.02	0.31 ± 0.02
3	1.29 ± 0.02	0.56 ± 0.03	0.60 ± 0.03	1.16 ± 0.04	0.30 ± 0.02	0.32 ± 0.02
5	1.28 ± 0.02	0.52 ± 0.03	0.54 ± 0.03	1.15 ± 0.02	0.31 ± 0.02	0.36 ± 0.02
7,5	1.28 ± 0.01	0.54 ± 0.02	0.63 ± 0.03	1.16 ± 0.04	0.33 ± 0.03	0.40 ± 0.03
10	1.31 ± 0.02	0.51 ± 0.03	0.60 ± 0.03	1.16 ± 0.03	0.38 ± 0.03	0.43 ± 0.03
15	1.28 ± 0.02	0.42 ± 0.02	0.45 ± 0.04	1.17 ± 0.04	0.40 ± 0.03	10.47 ± 0.03
		G series—ZrO_2 matrix			G series—Al_2O_3 inclusions	
1	1.28 ± 0.01	0.64 ± 0.04	0.73 ± 0.04	1.08 ± 0.02	0.18 ± 0.02	0.19 ± 0.02
3	1.29 ± 0.02	0.59 ± 0.03	0.66 ± 0.03	1.06 ± 0.01	0.17 ± 0.01	0.18 ± 0.01
5	1.28 ± 0.02	0.51 ± 0.03	0.60 ± 0.03	1.08 ± 0.02	0.16 ± 0.02	0.18 ± 0.02
7,5	1.27 ± 0.01	0.46 ± 0.03	0.48 ± 0.03	1.05 ± 0.02	0.16 ± 0.01	0.18 ± 0.02
10	1.28 ± 0.02	0.44 ± 0.03	0.50 ± 0.03	1.06 ± 0.01	0.17 ± 0.01	0.20 ± 0.01
15	1.28 ± 0.02	0.40 ± 0.02	0.42 ± 0.03	1.07 ± 0.02	0.18 ± 0.02	0.21 ± 0.02

[a]Ratio of a circumference of the grain cross-section to that of a circuit of the same area.

indicate that both the matrix grains and the inclusions were isometric in shape. The lack of statistically essential differences between the Feret diameters in the X and Y direction proves microstructural isotropy of the composites. Moreover, the comparison of the inclusion shape coefficients for both series of the composites shows that the inclusions derived from the γ-Al_2O_3 micropowder were spherical (shape coefficient does not differ essentially from unity) whilst those derived from the α-Al_2O_3 powder had near-polyhedron shape (shape coefficient >1).

The influence of chemical composition and microstructural features on mechanical properties of the cubic zirconia—alumina composites is shown in Figs 5–8. Fig. 5 illustrates the changes of hardness as a function of aluminium oxide content in the composites and their porosity. The dashed line in Fig. 5 is drawn based on the assumption that the rule of mixture can be used to determine the expected hardness of the studied composites. At any addition level, the experimental

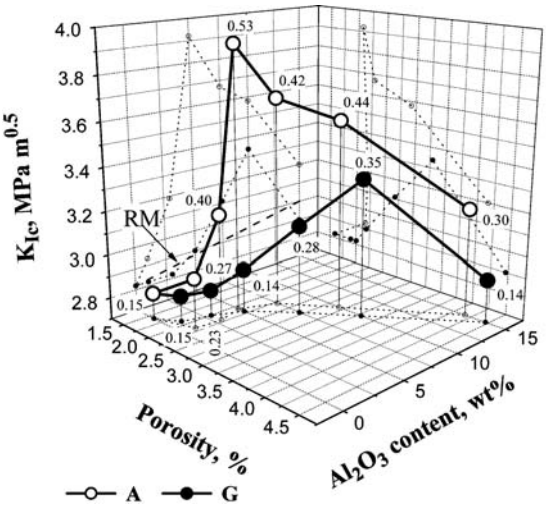

Figure 6 Critical stress intensity factor as a function of alumina content and porosity of the composites. The points are labelled with a confidence interval of K_{Ic} at confidence level of 0.95. A dashed line is calculated from the rule of mixture using the K_{Ic} values of 2.8 MPa·m$^{0.5}$ and 4.1 MPa·m$^{0.5}$ for cubic zirconia and alumina [31], respectively.

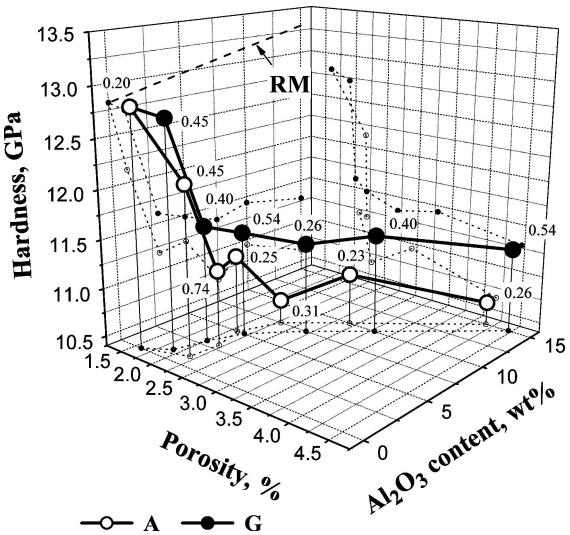

Figure 5 Vickers hardness as a function of alumina content and porosity of the composites. The points are labelled with a confidence interval of HV at confidence level of 0.95. A dashed line is calculated from the rule of mixture using the HV values of 12.8 GPa and 16 GPa for cubic zirconia and alumina [31], respectively.

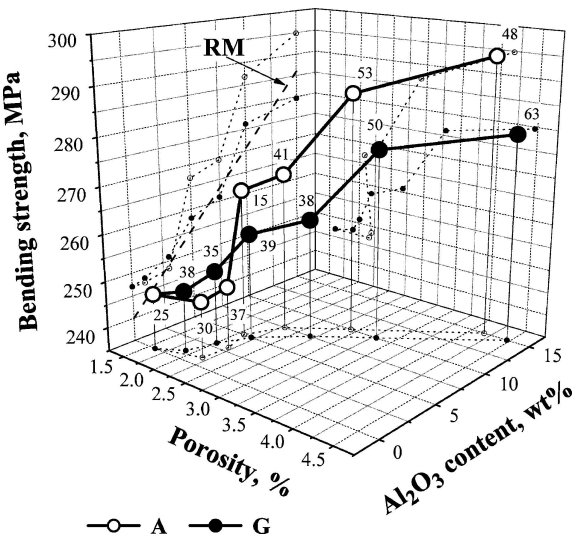

Figure 7 Bending strength as a function of alumina content and porosity of the composites. The points are labelled with a confidence interval of σ_f at confidence level of 0.95. A dashed line is calculated from the rule of mixture using the σ_f values of 240 and 550 MPa for cubic zirconia and alumina [31], respectively.

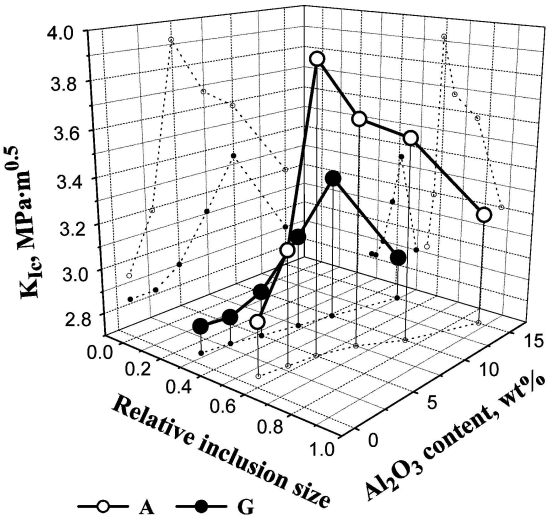

(a)

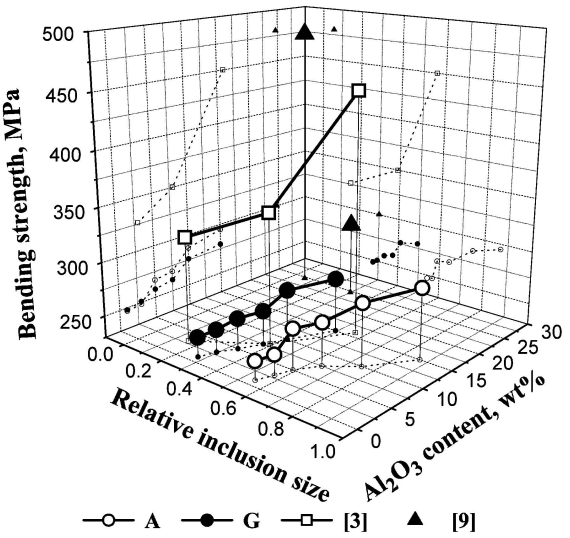

(b)

Figure 8 Influence of the relative inclusion size and alumina content on (a) fracture toughness and (b) bending strength of the cubic zirconia-alumina composites. Squares are data from Esper *et al*. [3]; solid triangles are data from Oe *et al*. [9].

results are lower than the expecting line. The addition of 5 wt% aluminium oxide caused a decrease in hardness of the materials (about 10% in maximum) and despite of the further increase of the inclusion content, hardness did not change significantly. The changes in hardness were slightly smaller in the case of composites with smaller alumina inclusions—the *G* series. The reason of such behaviour is a strong dependence of hardness of the composites on their porosity what is also shown in Fig. 5. The large decrease in hardness (about 20%) accompanied small increase in porosity of the composites from 1.5 to 2%. The composites with densities smaller than 98% did not show further dramatic decrease in hardness. As a number of inclusions per volume unit, which influences homogeneity of their distribution, was larger in the composites derived from the fine-grained alumina powder (*G* series) than in those derived from the coarse-grained powder (*A* series), the former materials showed higher hardness despite of larger porosity.

Fig. 6 shows fracture toughness of the studied composites as a function of porosity and alumina phase content. The dashed line in this figure illustrates predictions of the rule of mixture. At any addition level, the experimental results are larger than the expected ones showing similar course for both series studied. It shows a maximum which depended on the size of alumina inclusions. The maximum value of fracture toughness was reached at 5 and 10% alumina inclusions for the composites of the *A* and *G* series, respectively. The increase of fracture toughness of the composites was present independently on the increase of porosity up to ∼3%. Further increase of porosity deteriorated this property of the composites. As shown by Choi *et al.* [11], fracture toughness increases up to 24.7 wt% alumina addition in fully dense cubic zirconia-alumina composites.

Changes in bending strength of the cubic zirconia-alumina composites with reinforcement content and porosity are shown in Fig. 7. The values coming from the rule of mixture are marked with dashed line in the figure. A linear increase in bending strength with alumina content was observed for both series of the composites despite of increasing porosity. Presenting lower porosities, the *A* series composites showed higher strengths than those of the *G* series and of predictions made on the base of the rule of mixture. However, it should be emphasised that the latter ones are strongly dependent on the strength values taken to the calculations. The presented results are very similar to those obtained by Mori *et al.* [7].

In order to analyse the influence of alumina inclusion size on fracture toughness and strength of the composites independently on the zirconia matrix grain size, the values have been plotted as a function of relative inclusion size as shown in Fig. 8a and b. The relative inclusion size was defined as the ratio of the average alumina inclusion size and the average zirconia matrix grain size. The 3D trajectory graph in Fig. 8a and b shows also a dependence of K_{Ic} or σ_f on the alumina inclusion content.

The trajectories indicate that both fracture toughness and strength of the cubic zirconia-alumina composites with homogeneously dispersed isometric alumina inclusions is not a simple function of the relative inclusion size in the 0–1 range at a constant alumina content. Both the data obtained in the presented experiments and those taken from literature [3, 9] show that the dependence on relative inclusion size is connected first of all with the preparation method applied which should be seen as the dependence on whole composite microstructure obtained. This include in minor extent the inclusion size but more the other microstructural features i.e. grain size, porosity, pore size distribution, inclusion content and their location with respect to the other components of the microstructure.

The above presented observations can be explained by using the well-established Griffith equation [32] which describes relation between fracture toughness, K_{Ic}, and fracture strength, σ_f, of brittle materials:

$$\sigma_f = \frac{K_{Ic}}{Y\sqrt{\pi a}} \tag{2}$$

where a is the length of the flaw and Y is a geometry factor approximately equal to 1.

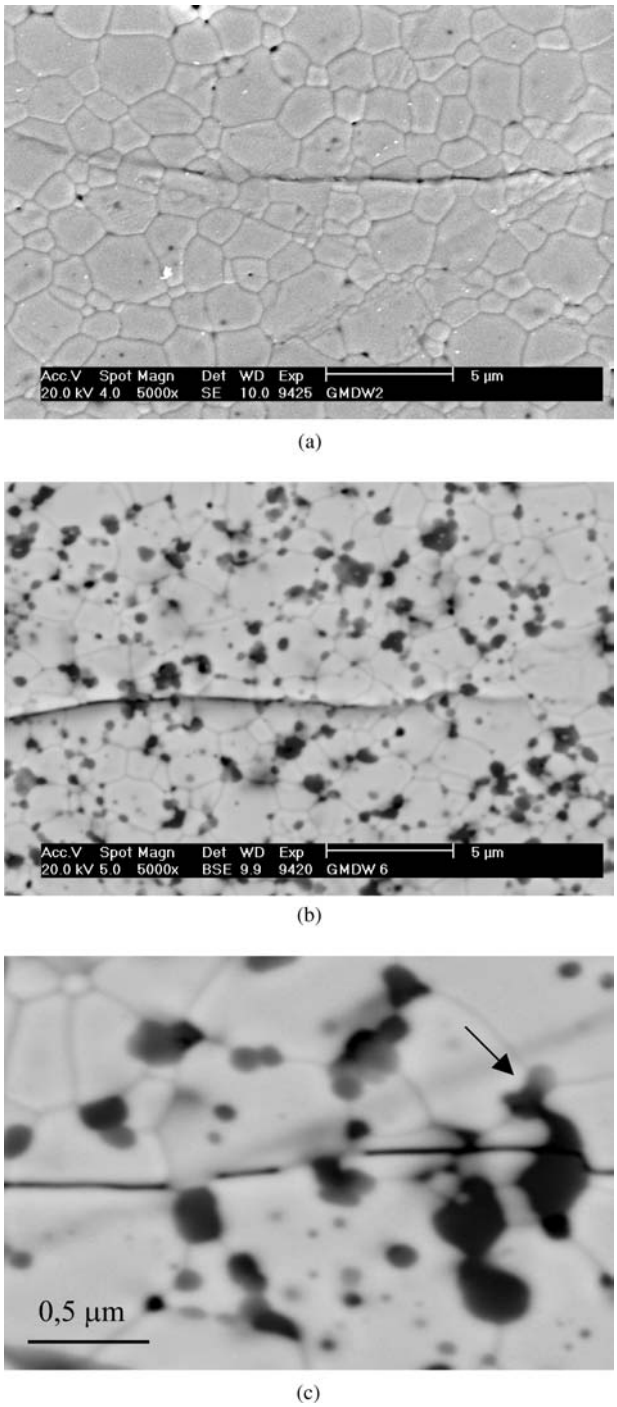

Figure 9 SEM microphotographs of the crack propagation through: (a) cubic zirconia, (b) G10 composite and (c) A10 composite.

According to this equation as long as the inclusion is not identified with the flaw of critical size and K_{Ic} remains constant the inclusion size dependence of fracture strength will not be observed. However, if the inclusion size affects fracture toughness of the material without influencing the critical flaw size, the strength will change. The latter seems to be the case. The zirconia grains (Fig. 4) and pores (Fig. 2) had the larger size than that of the alumina inclusions and therefore they have been the most probable source of the critical flaw in the zirconia-alumina composites of relative inclusion size <1. Even though the critical flaw size to cause failure may not scale with the alumina inclusion size itself, the formation probability of it depended on the alumina inclusions through their influence on porosity. Taking above into the consideration, the increase of strength of the A series composites should be attributed to two effects connecting with the incorporation of alumina inclusions and predicted by the Equation 2: (i) a reduction in the flaw size by the better densification which favours reduction in the pore sizes; (ii) increasing fracture toughness by processes that shield the crack tip from the applied stress [33].

The increase in fracture toughness accompanied by the incorporation of alumina is ascribed to the crack deflection due to the residual compressive stress derived from inter-granular alumina. The SEM investigation of cracks propagated through the studied materials (Fig. 9) revealed differences between crack paths depended on the alumina inclusion size.

In the cubic zirconia material with any alumina inclusions, the cracks propagated both along the grain boundaries and across the zirconia grains (Fig. 9a). Deflection of the crack path is only related to the curvature of the grain boundaries. In the *G* series composite with fine alumina inclusions, a similar crack path has been found in the zirconia grains area (Fig. 9b). Encountering alumina inclusions, the crack propagated along the interfaces. The interaction of the crack with the grain boundaries and interfaces caused the deflection effect.

In the case of the A10 composite which contained coarse inclusions, cracking across the alumina grains was observed as an additional process increasing the reduction in stress intensity. Fig. 9c shows the crack which after reaching the coarse alumina grain (indicated by arrow) significantly deflects and further it goes along the interface almost perpendicular to the original direction. The alumina grain did not crack until the crack tip reached a cross section at which the energy of elastic strains accompanied the propagating crack exceeded the tensile strength of the grain. The probability of such event increases with an increase of the size and the content of the inclusions. This contribution of the large grains to the crack deflection mechanism explains the larger increase of K_{Ic} observed in the case of the *A* series composites when compared to that observed in the case of the *G* series composites which contained almost two times smaller alumina inclusions.

4. Summary and conclusions

An investigation shown in the paper indicates that mechanical properties of the cubic zirconia-alumina composites are affected by inclusion content, inclusion size, porosity and distribution of the inclusions. It is difficult to prepare the composites in that the effect of inclusion size can be analysed separately from other factors. So, the relationship between mechanical properties and the relative inclusion size is strongly dependent on the preparation method applied.

The method applied in the study was suitable for the production of cubic zirconia–alumina composites with submicron alumina inclusions dispersed homogeneously with the submicron zirconia matrix. The inclusions were mainly located in the zirconia grain boundaries. The application of zirconia nanopowder with excellent sinterability enabled to produce the composites

containing up to 5 wt% alumina with good densification (98%) at the temperature as low as 1300°C by pressureless sintering.

The microstructure of the cubic zirconia—alumina composites was composed of isometric grains both of the matrix and the inclusions. The latter ones receive shape which is dependent on the original alumina particle size. It changes from polyhedral for the big alumina inclusions (0.35 μm) to spherical for the fine ones (0.18 μm).

The incorporation of alumina particles to the cubic zirconia powders deteriorates their densification during sintering the stronger the smaller is the alumina particles size and the larger is their content. It makes difficult to produce the cubic zirconia of improved hardness. However, the composites with smaller alumina inclusions presented higher hardness.

For the materials of density of +97%, an increase in fracture toughness of the composites was detected. It was dependent on the alumina size. A contribution from the big alumina inclusions to the crack deflection mechanism has been found.

Decreasing the inclusion size significantly below the submicron matrix grain size (more than 3 times) does not lead to improvement of fracture toughness and strength of the composites.

Acknowledgements

The work was supported by the State Committee for Scientific Research under the grant no. 7 T08D 014 11.

References

1. B. Q. MINH, *J. Amer. Ceram. Soc.* **76** (1993) 563.
2. E. P. BUTLER and J. DRENNAN, *ibid.* **65** (1982) 474.
3. F. J. ESPER, K. H. FRIESE and H. GEIER, in "Science and Technology of Zirconia," edited by N. Claussen, M. Rühle and A. H. Heuer (American Ceramic Society, Columbus, OH, 1984) p. 528.
4. S. RAJENDRAN, J. DRENNAN and S. P. S. BADWAL, *J. Mat. Sci. Lett.* **6** (1987) 1431.
5. X. GUO, C.-Q. TANG and R.-Z. YUAN, *J. Europ. Ceram. Soc.* **15** (1995) 25.
6. M. MIYAYAMA, H. YANAGIDA and A. ASADA, *Am. Ceram. Soc. Bull.* **64** (1986) 660.
7. M. MORI, T. ABE, H. ITOH, O. YAMMAMOTO, Y. TAKEDA and T. KAWAHARA, *Solid State Ion.* **74** (1994) 157.
8. P. DURAN, L. M. NAVARRO, P. RECIO and J. R. JURADO, *Eur. J. Solid State Inorg. Chem.* **32** (1995) 963.
9. K. OE, K. KIKKAWA, A. KISHIMOTO, Y. NAKAMURA and H. YANAGIDA, *Solid State Ion.* **91** (1996) 131.
10. P. BHARGAVA and B. R. PATTERSON, *J. Amer. Ceram. Soc.* **80** (1997) 1863.
11. S. R. CHOI and N. P. BANSAL, *Ceram. Eng. Sci. Proc.* **23** (2002) 741.
12. W. PYDA, K. HABERKO and M. M. BUĆKO, *J. Amer. Ceram. Soc.* **74** (1991) 2622.
13. K. NIIHARA, *J. Mat. Sci. Lett.* **2** (1983) 221.
14. A. G. EVANS, *J. Amer. Ceram. Soc.* **65** (1982) 497.
15. G. W. SCHERER, *ibid.* **67** (1984) 709.
16. R. RAJ and R. BORDIA, *Acta Metall.* **32** (1984) 1003.
17. C. H. HSUEH, *J. Mater. Sci.* **21** (1986) 2067.
18. C. H. HSUEH, A. G. EVANS, R. M. CANNON and R. J. BROOK, *Acta Metall.* **34** (1986) 927.
19. R. K. BORDIA and G. W. SCHERER, *ibid.* **36** (1988) 2392.
20. F. F. LANGE, *J. Mater. Res.* **2** (1987) 59.
21. S. SUNDARESAN and I. A. AKSAY, *J. Amer. Ceram. Soc.* **73** (1990) 54.
22. O. SUDRE, G. BAO, B. FAN, F. F. LANGE and A. G. EVANS, *ibid.* **75** (1992) 525.
23. F. F. LANGE and M. M. HIRLINGER, *ibid.* **70** (1987) 827.
24. F. F. LANGE, T. YAMAGUSHI, B. I. DAVIS and P. E. D. MORGAN, *ibid.* **71** (1988) 446.
25. B. J. KELLETT and F. F. LANGE, *ibid.* **72** (1989) 725.
26. F. F. LANGE and B. J. KELLETT, *ibid.* **72** (1989) 735.
27. M. W. WEISER and L. C. DE JONGHE, *ibid.* **71** (1988) C-125.
28. A. NAKAHIRA and K. NIIHARA, *J. Ceram. Soc. Jpn.* **100** (1992) 448.
29. D. A. PORTER and K. E. ESTERLING, in "Phase Transformations in Metals and Alloys," 2nd edn. (Chapman & Hall, London, 1992) p. 139.
30. M. KLEITZ, L. DESSEMOND and M. C. STEIL, in Proceedings of SOFC; Materials, Process Engineering and Electrochemistry, Fifth IEA Workshop, edited by P. Biedermann and B. Krahl-Urban, (Julich, 1993) p. 147.
31. W.E. LEE and W. M. RAINFORTH, in "Ceramic Microstructures, Property Control by Processing" (Chapman & Hall, London, 1994) p. 278.
32. B. LAWN, in "Fracture of Brittle Solids," 2nd edn. (Cambridge, UK, 1993).
33. I. E. REIMANIS, *Mater. Sci. Engng.* **A237** (1997) 159.

Received 23 January
and accepted 17 December 2004